Title

BEHAVIOR IN MAGNETIC FIELD AND SPATIAL RESOLUTION OF A DRIFT CHAMBER WITHOUT ELECTRIC FIELD SHAPING

Authors

Sadoulet, B.
Lithe, A.

Publication Date

1974-08-01

Submitted to Nuclear Instruments and Methods

LBL-3316
Preprint

BEHAVIOR IN MAGNETIC FIELD AND SPATIAL RESOLUTION OF A DRIFT CHAMBER WITHOUT ELECTRIC FIELD SHAPING

B. Sadoulet and A. Litke

August 1974

Prepared for the U. S. Atomic Energy Commission
under Contract W-7405-ENG-48

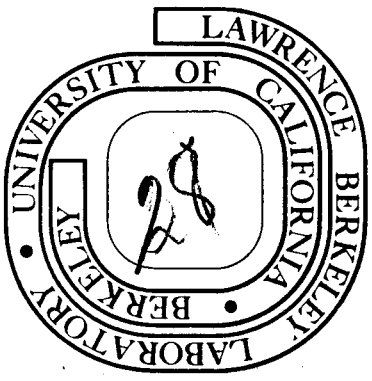

DISCLAIMER

Submitted to Nuclear Instruments and Methods
LBL-3316

BEHAVIOR IN MAGNETIC FIELD AND SPATIAL RESOLUTION OF A DRIFT CHAMBER WITHOUT ELECTRIC FIELD SHAPING*

B. SADOULET and A. LITKE

University of California, Lawrence Berkeley Laboratory
Berkeley, California 94720, USA

ABSTRACT

We present results on the behavior in a magnetic field parallel to the sense wires and the spatial resolution of a drift chamber with relatively short drift length (7.52 mm) but without electric field shaping. This chamber operates quite well for a field as high as 15 kilogauss, and the spatial resolution is better than ±100 μm over the major part of the chamber for normally incident tracks. At 4 kg we give results on the spatial resolution as a function of the incident angle.

---

*This work was performed under the auspices of the U. S. Atomic Energy Commission.

1. Introduction

Multiwire drift chambers[1-6] have aroused remarkable interest recently, especially as very accurate particle position detectors. After the pioneering work of Charpak et al.,[1] Walenta and co-workers[3] built very simple drift chambers: to the sense wires and cathodes of an ordinary multiwire proportional chamber they added field wires between the sense wires in order to suppress regions of zero electric field (see fig. 1). These types of chambers with a drift length of 0.5 cm have been used in actual experiments in magnetic fields of up to 7 kG. However, no detailed study of the ultimate spatial resolution of such chambers has, as yet, been made.

Charpak, Sauli and co-workers[2] recently made a very careful study of the spatial resolution of another type of drift chamber in which the electric field is shaped in such a way that the electrons drift in a quasi homogeneous field. With a drift length of 2.5 cm they obtained resolutions better than 150 μm. Behavior in a magnetic field was also studied systematically and the possibility of operation at 15 kG was demonstrated at the price, however, of tilting the electric field in the gap.

Field shaping may be impractical mechanically for large chambers[4] or for cylindrical geometry applications in which the present authors are interested. For a cylindrical chamber one would like to simplify the already complex construction as much as possible. Moreover, field shaping strips on the cathodes have to be parallel to the wires and are incompatible with a simple readout of the longitudinal coordinate. One is obliged to use individual delay line readout[7] -- a rather complex

scheme -- instead of simply using the signal induced on cathode strips which make an angle with the wires. Note that in the latter method, timing of the cathode signals provides (like the first method) a pairing of the azimuthal and longitudinal coordinates.

The question arises then whether the same resolution and good behavior in a magnetic field parallel to the sense wires can be obtained in the simpler chambers of the Walenta type or whether careful field shaping is in fact essential for good results.

In this article we will show that good results can be obtained with chambers without field shaping for a relatively small drift length (7.5 mm).

Section 2 describes our test chambers and our test setup. In Section 3 we comment on the efficiency and the known defect[8] of chambers of the Walenta type to operate close to the semi-Geiger mode. Section 4 is devoted to the space/time relation and stability. Section 5 discusses the resolution obtained.

2. Test Setup

Figure 1 shows the type of chamber we have tested: the distance between sense wires is 1.52 cm. The sense wires are made of stainless steel with a diameter of 20 μm; the gold plated tungsten field wire diameter is 100 μm. The half gap is 4.19 mm. The cathodes have been made of copper strips about 1 mm wide, placed parallel to the wires and printed on mylar. This was to enable us to shape the electric field if it had been necessary. Each chamber had three active wires and an active area of about 5 × 4.5 cm.

We used a mixture of 66% argon, 30% isobutane and 4% methylal -- the same mixture that has been used by Charpak and co-workers. Each sense wire was loaded directly onto a 50 Ω coaxial cable about 3 meters long and the signal was fed into an amplifier and discriminator. The effective discriminator threshold was varied during the tests between 660 and 330 μV.

In order to measure the interesting parameters (especially the resolution) it is necessary to use a beam preferably of minimum ionizing particles. In our case, schedule requirements obliged us to use a beam of 1.39-GeV/c protons, which are unfortunately about 1.2 times minimum ionizing.

We used a method very similar to the one used by Charpak, Sauli and Duinker. Two chambers defined a well collimated beam. A third chamber was located between them and could be displaced with a micrometric movement. Figure 2 gives a diagram of the fast logic used. It is essentially straightforward. In order to increase the rate, the two external chambers A and C, in very tight coincidence (± 1.5 ns), were allowed to have a time jitter of ± 10 ns with respect to the scintillators which defined the beam. This corresponds to an effective beam width of 1 mm. For a beam that passes on the same side of the sense wires in all chambers the effect of the width of the beam cancels in the resolution measurement provided that the drift velocity is the same in the three chambers. Unfortunately this was not always true and obliged us to introduce corrections which increased the uncertainty in the resolution (see Appendix I). Note also in fig. 2 that we had the possibility of "ORing" two wires of the intermediate chamber B in order to study the transition region in the vicinity

of the field wire.

3. Efficiency

3.1 Electric Field Configuration in Drift Chambers of Walenta's Type

Before describing our results on efficiency we should comment on the electric field configuration in drift chambers of Walenta's type. Figure 1(a) gives the field lines (dotted lines) in our chambers when the cathode is at -2050 V with respect to the sense wires and the field wires are at -560 V relative to the cathode.† It is necessary to put the field wires at such a negative voltage ΔV with respect to the cathode in order to sufficiently increase the electric field in the drift region between the field wire and the sense wire (see Section 4). The consequence is that some field lines go from the field wire to the cathode and that there are four "pockets" of very small field around the field wire. Therefore, for tracks passing very close to the field wire only a small fraction of the primary electrons deposited may be used and since their density is relatively small (about 30/cm of track; see for instance ref. 10) one may expect an inefficiency close to the field wire increasing with $|\Delta V|$.‡

In order to minimize this effect, the avalanche amplification should be such that the electronics are sensitive to one primary electron.

---

†The electric field has been computed with a modified version of a computer program kindly provided to us by F. Bourgeois and J. P. Dufey.[9]

‡The authors of ref. 6 have proposed to get rid of this effect by using foils instead of field wires. This solution seems, however, too complicated for our cylindrical geometry.

If the electronic threshold is too high, one cannot reach this region without entering into a semi-Geiger region for some avalanches, especially those corresponding to tracks closer to the sense wire. This mode is characterized by longer pulses [compare fig. 3(b) to fig. 3(a)] and a very long deadtime due to an ion coating around the wire.[8]

Note that the problems associated with the low density of useful electrons deposited near the field wire may also be present in chambers with field shaping. However with a large drift length the importance of the relevant region is proportionally much smaller.

3.2 Plateau Curves

Figure 4(a) gives efficiency curves as a function of high voltage under several conditions for tracks about 5 mm from the sense wire. Figure 4(b) gives the logarithm of the corresponding singles rate on the wire. Several features may be noted:

a) The drop of efficiency at high voltage cannot be caused by the deadtime of our electronics. It corresponds to the appearance of "semi-Geiger" pulses in the sense defined above and we think that these are responsible for this effect.

We seem to be more sensitive to this effect than Charpak, Sauli and co-workers[2] who are able to have pulses of 3 mV on 50 Ω with the same gas without any Geiger pulses. This cannot be an effect of the geometry since the breakdown point is presumably only related to the total charge in the avalanche or equivalently the pulse height. This may be due to the nature of our sense wires or poor cleanliness of the chamber.

b) Between low (300 particles/sec) and high rates (80 k particles/second), there is a displacement of the plateau. This is presumably due to space charge effects caused by ions drifting in the gap.[11]

c) There is only a minor influence of ΔV on the pulses as expected from electrostatic calculations.

3.3 Efficiency as a Function of Position

Figure 5(a) gives the efficiency as a function of position of the beam at zero magnetic field for various ΔV at a relatively high threshold of 660 μV. In most of the chamber the efficiency is compatible with 99% or better[§] except in the region of the field wire where we observed a very dramatic drop (note that the scale begins at 80%). This shows that our threshold was not low enough (since we are limited in high voltage by Geiger pulses). Only a small dependence on ΔV, if any, is observed.

We have studied in more detail the effect of the threshold at 4 kG since we are mainly interested in that magnetic field region for the application we have in mind. Figure 5(b) shows that a threshold of 330 μV gives for ΔV = 560 V an inefficiency of 2% for a beam 1 mm wide centered on the field wire. This corresponds to an equivalent totally dead region of 20 μm.

At larger fields one may be worried by the distortion of trajectory exemplified for 15 kG in fig. 1(c). The assumption used in this figure

---

[§]The indication of a slight drop close to the sense wire may not be significant. We have found no explanation for it.

of a drift velocity along the electric field unaffected by the magnetic field and of a magnetic drift velocity equal to the drift velocity are known to be too optimistic[10] and one may be worried that the trajectories of some electrons come too close to the cathodes and that we lose some efficiency at large drift distance. Figure 5(c) shows that this is not the case.

In conclusion, our measurement shows that the efficiency is not affected drastically by the magnetic field between 0 and 15 kG, and that a threshold of 330 μV gives us a reasonable efficiency around the field wire.

4. Time Versus Position Curves

4.1 Dependence on ΔV at Zero Magnetic Field

We show in fig. 6 the dependence of the electron drift time on the position of tracks normal to the chamber for four values of the potential differences ΔV between the field wire and the cathode. When ΔV = 0 the relation is very nonlinear. Increasing ΔV corrects this partially but even when a ΔV as high as 1124 V is applied there is still a slight non-linearity.

Figure 7 gives the electric field along the center line of the chamber as a function of the distance from the sense wire. Using these curves and the values of the drift velocities obtained from a polynomial fit to our measurements,[Π] we get the dependence of the drift velocity on

[Π] We disregarded the points close to the field wire since a primary electron not produced exactly at the center of the chamber will have a much larger path length as shown in fig. 1(a).

the electric field shown in fig. 8(a). It should be noted that the drift velocity obtained from our gas mixture saturates much later than the drift velocity measured by Charpak and co-workers for a mixture of 30% isobutane and argon. It is possible that this is due to the presence of methylal which may cool down the electrons and push away the saturation point.[10] Unfortunately we cannot tell exactly at what field the saturation begins from our measurement. The authors of ref. 2 claim that at 1400 V/cm they are inside the saturation region with, in principle, the same gas as ours. This is not incompatible with our measurement.

The problem with our space time relation is not its nonlinearity, which can be corrected by software, but the fact that we are using a region of electric field where the dependence of drift velocity is quite steep; it may then be quite difficult to maintain a good stability of the drift velocity. Mechanical imperfection of the chambers, difference in temperature or in high voltage will then spoil the good resolution of this chamber. The obvious remedy is to increase the gap width, for instance, to 6 mm. One may compute that with a ΔV of 1450 volts and suitable voltage on the cathode in order to have the same amplification ($V = 2250$), the shape of field lines around the field wire is very similar to the one obtained in our case for $\Delta V = 560$ and that the minimum field in the gap along the center line is 1400 V/cm. This should be sufficient for stability according to the authors of ref. 2.

4.2 Dependence on the Magnetic Field

Figure 9 shows the dependence of the electron drift time on spatial position for three values of magnetic field parallel to the wires.

It can be seen easily that in the approximation that the drift velocity along the electric field is independent of the magnetic field,[¶] then the space time relation should remain approximately the same.

With obvious notation, in polar coordinates (fig. 10) we have:

$$\frac{dr}{dt} = w_{||}(E,B) \simeq w_{||}(E,B=o)$$

$$r\frac{d\psi}{dt} = w_{\perp}(E,B) = w_m(E,B)\frac{B}{E}$$

where $w_{||}$ and $w_{\perp}$ are the drift velocities parallel and perpendicular to the electric field, and w_m is the magnetic drift velocity which is of the same order as w.[10] Because of the focusing effect of the nearly radial electric field, ψ is always small (see fig. 1(c)) and to first approximation

$$\frac{dx}{dr} = \frac{d(r\cos\psi)}{dt} \simeq \frac{dr}{dt} = w_{||}(E,B) \simeq w_{||}(E,B=o)$$

Therefore the space time relationship should remain unchanged.

At 4 kG this is very nearly the case. The drift velocity is hardly changed also as shown in fig. 8(b). At 15 kG the magnetic field is high enough to significantly cool down the electrons (see ref. 10), the drift velocity is much smaller (fig. 8(c)) and the time space relation is much steeper.

4.3 Dependence on the Angle

At 4 kG, which is the region of magnetic field that we are

[¶]This assumption is correct for sufficiently small magnetic fields. See ref. 10.

interested in, we have measured the dependence of the space time relation on the angle of the incident track. Our angle convention is given in fig. 10(b) and the results are given in fig. 11.

In principle the magnetic field introduces an asymmetry into the problem and positive and negative angles should give slightly different results. Simulation however, shows that the difference is very small at 4 kG and in this preliminary investigation we have not measured this effect.

5. Spatial Resolution

We arrive finally at the main question this paper tries to answer: "What is the intrinsic resolution of this kind of drift chamber?"

Appendix I describes the formalism we have used in order to derive the chamber resolution. The results of this elaborate method differ by 20% from the simple-minded approach where one simply writes

$$\sigma_x = \sqrt{\frac{2}{3}} w \, \sigma_t$$

where σ_t is the measured rms of the time distribution (B - A) and w is the drift velocity. In fact our results are limited in accuracy by the poor knowledge we have of the drift velocity** which is important in order to compute the effect of a wide beam on the resolution.

**A simple time spectrum without collimation would have solved this problem.

5.1 Resolution at Zero Magnetic Field

Figure 12 gives the spatial resolution at zero magnetic field for various ΔV. The threshold is 660 μV. We may compare these results to what was expected:[10]

a) In the region close to the sense wire, the resolution should be limited by the dispersion of primary electrons and an rms resolution of about 130 μm is expected on the wire (our incident tracks are not minimum ionizing). We have not measured the resolution close enough to the sense wire to actually see this effect but our results are compatible with that expectation.

b) Further from the wire, the dominant effect should be the diffusion of electrons. This would give a resolution which is proportional to the square root of the distance. From the results of the authors of ref. 2, who give a resolution of 130 μm at 2 cm for the same gas, we expect at 5 mm a resolution of about 65 μm. This is in agreement with our measurement.[††]

c) Close to the field wire, the resolution may be degraded by the increased time slewing due to the smaller pulse height. With our relatively high threshold of 660 μV, we observe this effect and our time distribution in the field wire region is skewed. At 4 kG, however, with a smaller threshold of 330 μV, this effect disappears.

[††] They do not quote 65 μ at 5 mm because they have not subtracted the contribution of their electronics.

5.2 Resolution as a Function of Magnetic Field

Figure 13 shows the spatial resolution as a function of position for different magnetic fields. These results are for normally incident particles. Unfortunately the zero magnetic field results have been obtained with a threshold of 660 μV while the other results correspond to a threshold of 330 μV. We may however conclude that a 4 kG the resolution is not degraded and that even at 15 kG the resolution is better than 100 μm.

5.3 Resolution as a Function of Angle

Figure 14 gives the chamber resolution as a function of the angle of the incident track at 4 kG. While the resolution is compatible until 5 mm with the fact that we are measuring the distance of closest approach, we observe some degradation for large angle tracks close to the field wire.

6. Conclusion

The results of this preliminary study are very encouraging. We obtained good efficiency even in the region of the field wire (for low enough threshold), good behavior in magnetic fields as high as 15 kG, and a spatial resolution better than 75 μm over most of the chamber.

Clearly, before using such a device in an experiment requiring this full accuracy, some modifications are needed: We will especially try to push further the semi-Geiger region (cleaning the wires or going to gold-plated tungsten), and we will increase the gap in order to operate in a higher electric field and obtain a better stability of the drift velocity. Careful calibration obviously is also necessary.

ACKNOWLEDGMENTS

One author (B.S.) is very grateful to G. Charpak and F. Sauli for the numerous conversations about drift chambers and this project. We would also like to acknowledge valuable discussions with D. Nygren, A. Wagner, and A. Walenta. We are grateful for the work of the technicians of our group for their fine construction work, and thank especially N. Andersen, P. Harding, E. Lee, and G. Smith.

REFERENCES

1. G. Charpak, D. Rahm and H. Steiner, Nuclear Instr. Methods 80, (1970) 13.

2. G. Charpak, F. Sauli, W. Duinker, Nuclear Instr. Methods 108, (1970) 613. A. Breskin, G. Charpak, B. Gabioud, F. Sauli, N. Trautner, W. Duinker, G. Schultz, "Further results on the operation of high accuracy drift chamber," CERN preprint, (Feb. 1974).

3. A. H. Walenta, J. Heintze, B. Schurlein, Nuclear Instr. Methods 92, (1971) 373. J. Heintze, A. H. Walenta, Nuclear Instr. Methods 111, (1973) 461. A. H. Walenta, Nuclear Instr. Methods 111, (1973) 467.

4. D. C. Cheng, W. A. Koranecki, R. L. Piccioni, C. Rubbia, L. R. Sulak, W. J. Weedon and J. Whittaker, "Very large proportional drift chambers with high spatial and time resolutions," Harvard preprint (1973).

5. R. Chaminade, J. C. Duchazeaubeneix, C. Laspalles, and J. Saudinos, Nuclear Instr. Methods 111 (1973) 77.

6. M. Atac and W. E. Taylor, "The development of a new drift chamber with a new gas mixture," NAL preprint (Feb. 1974) NAL-Pub-74/22-EXP.

7. A. Breskin, G. Charpak, F. Sauli and J. C. Santiard, "Two-dimensional drift chambers," submitted to Nuclear Instr. Methods, CERN preprint (Dec. 1973).

8. F. Sauli, private communication.

9. F. Bourgeois and J. P. Dufey, "Programmes de simulation des chambres à drift," CERN internal report (unpublished) (July 1973).

10. V. Palladino and B. Sadoulet, "Application of the classical theory of electrons in gases to multiwire proportional and drift chambers," Lawrence Berkeley Laboratory Report LBL-3013 (1974). A shorter version (LBL-3070) has been submitted for publication.

11. L. Cohen, C. Grunberg, and J. deDevechat, Nuclear Instr. Methods 103, (1972) 125. B. Sadoulet and B. Makowski, "Space charge effects in multiwire proportional counters," CERN preprint, CERN/D.Ph.II/PHYS 73-3.

APPENDIX 1
CALCULATION OF THE RESOLUTION

Let us call x_A^o the position of a beam track in chamber A, x_A the position as deduced from the measured time, x_A^C the central position of the beam, and x'_A the drift velocity at this position. The position errors from the chamber are noted σ_A ($\sqrt{<\sigma^2_A>}$ = the position r.m.s.), and the electronic noise contribution to the time error is τ_A. We have then

$$x_A - x_A^o = \sigma_A + \tau_A x'_A$$

We use similar notations for chambers B and C.

Chambers A and C are put in tight coincidence of half with δt_{max}. This is expressed by the equation

$$\frac{x_C - x_C^C}{x'_C} - \frac{x_A - x^C_A}{x'_A} = \delta t$$

with $< \delta t^2 > = \frac{(\delta t_{max})^2}{6}$. Moreover they are required to be in coincidence of half width Δt_{max} with the scintillator. If $\Delta t_{max} >> \delta t_{max}$, we may then write

$$\frac{x_A - x^C_A}{x'_A} + \frac{x_C - x_C^C}{x'_C} = 2\,\Delta t$$

The track position in chamber B which is half way between A and C is

$$x^o_B = \frac{x_A^o + x_C^o}{2} + \delta s$$

where δs is the multiple scattering contribution.

From these various equations we may deduce

$$\frac{x_A^o - x_A^C}{x'_A} = \Delta t - \frac{\delta t}{2} - \frac{\sigma_A}{x'_A} - \tau_A$$

$$\frac{x^o_C - x_C^C}{x'_C} = \Delta t + \frac{\delta t}{2} - \frac{\sigma_C}{x'_C} - \tau_C$$

$$\frac{x^o_B - x^C_B}{x'_B} = \left(\frac{x'_A + x'_C}{2x'_B}\right)\Delta t + \frac{(x'_C - x'_A)}{4x'_B}\,\delta t - \frac{\sigma_A + \sigma_C}{2x'_B} - \frac{x'_A\tau_A + x'_C\,\tau_C}{2} + \delta s$$

$$\frac{x_A - x^C_A}{x'_A} = \Delta t - \frac{\delta t}{2}$$

Finally

$$\frac{x_B - x^C_B}{x'_B} - \frac{x_A - x_A^C}{x'_A} = \frac{\sigma_B}{x'_B} + \tau_B + \frac{\delta s}{x'_B} - \frac{\sigma_A + \sigma_C}{2x'_B} - \frac{(x'_A\,\tau_A + x'_C\,\tau_C)}{2x'_B} + \left(\frac{x'_A + x'_C}{2x'_B} - 1\right)\Delta t + \left(\frac{x'_C - x'_A}{2x'_B} + 1\right)\frac{\delta t}{2}$$

and the position r.m.s. $\sqrt{<\sigma_B^2>}$ is:

$$\left[x'^2_B\,(<\sigma_t^2> - <\tau_B^2>) - <\delta s^2> - \frac{<\sigma_A^2> + <\sigma^2_C>}{4} - \frac{x'^2_A <\tau_A^2> + x'^2_C <\tau^2_C>}{4} - \left(\frac{x'_A + x'_C}{2} - x'_B\right)^2 \frac{\Delta t^2_{max}}{6} - \left(\frac{x'_C - x'_A}{2} + x'_B\right)^2 \frac{\delta t^2_{max}}{12}\right]^{\frac{1}{2}}$$

where $\sqrt{<\sigma_t^2>}$ is the r.m.s. of the measured time spectrum

$\langle \sigma_A^2 \rangle$ and $\langle \sigma_C^2 \rangle$ can be calculated by equating them to $\langle \sigma_B^2 \rangle$ at the relevant position. In our case

$$\sqrt{\langle \delta s^2 \rangle} = 25\ \mu m$$

$$\Delta t_{max} = 11.5\ ns$$

$$\delta t_{max} = 1.5\ ns$$

$$\sqrt{\langle \tau^2_A \rangle} = \sqrt{\langle \tau_B^2 \rangle} = \sqrt{\langle \tau_C^2 \rangle} = 0.2\ ns$$

One sees that for $x'_A = x'_B = x'_C$ the contribution of the beam width determined by Δt is zero. Unfortunately in some of our measurements $\frac{x'_A + x'_C}{2}$ was different from x'_B and not very well known and this increased our uncertainty on the final result.

FIGURE CAPTIONS

Fig. 1. (a) Test drift chamber: the dotted lines represent field lines and therefore the trajectory of electrons at zero magnetic field. Full lines are loci of equal drift time to the sense wire. They are spaced by 20 ns. For this plot the cathode potential is 2050 V and the field wire potential is 560 V higher. The measured drift velocity has been assumed.
(b) Same plot at 4 kG. Dotted lines now represent only the trajectories of electrons. The drift velocity has been assumed unmodified by the magnetic field and the magnetic drift velocity has been assumed to be equal to the usual drift velocity.
(c) Same plot at 15 kG.

Fig. 2. Test set-up.

Fig. 3. (a) Normal pulses at V = -2200 V, DV = -1124 V for tracks about 5 mm from the sense wire. (Vertical scale: 660 μV per division, horizontal scale: 20 ns/dw, scope triggered by A, C, PM coincidence, low rate).
(b) Same condition but with a vertical scale of 2.60 mV per division and a longer exposure. One sees clearly "semi Geiger" pulses which are about 100 ns long.

Fig. 4. (a) Efficiency curves. Threshold is 660 μV. High rate curve for ΔV = 560 (1) corresponds to about 80×10^3 hits per second on the wire studied and is corrected for dead time (4% ± 1.5% correction). Low rate curves are given for ΔV = 560 (2) and ΔV = 1124 (3) and correspond to a few hundred counts per second.
(b) Logarithm of the ungated number of hits on the wire studied in both conditions.

Fig. 5. Efficiency as a function of position for ΔV = 0, V = -2100 V; ΔV = 560, V = -2050 V; ΔV = 752, V = -2014; ΔV = 1124, V = -2050.
(a) At zero magnetic field for various ΔV, threshold is 660 μV.
(b) At 4 kG for various thresholds, ΔV = 560 V. For the point on the field wire the two adjacent wires are read.
(c) At 15 kG for ΔV = 560 V and a threshold of 330 μV.

Fig. 6. Dependence of the electron drift time on the position for various values of ΔV. The tracks are normal to the chamber. The cathode potentials corresponding to each ΔV are the same as in Fig. 5.

Fig. 7. Electric field as a function of position along the center line of the chamber for various ΔV. The cathode potentials corresponding to each ΔV are the same as in Fig. 5.

Fig. 8. Drift velocity as a function of electric field as deduced from our measurements (a) at 0 magnetic field, (b) at 4 kG field, (c) at 15 kG field.

Fig. 9. Dependence of the electron drift time on the position for three values of magnetic fields. Tracks are normal to the chamber. V = 2050 Volt and ΔV = 560 volts.

Fig. 10. (a) Polar coordinates used in the paper. The origin is the sense wire. (b) Convention for measuring the track angle θ. The magnetic field goes into the figure.

Fig. 11. Dependence of the electron drift time on the position for three angles. Convention given in Fig. 10(b). Magnetic field is 4 kG. V = 2050 volts and ΔV = 560 volts.

Fig. 12. Spatial resolution at zero magnetic field for various ΔV. Corresponding values of the cathode potential are the same as in Fig. 5. Threshold is 660 μV. The solid line is drawn to guide the eye. Dotted line is what is expected from the diffusion as deduced from the results of Ref. 2.

Fig. 13. Spatial resolution for three magnetic fields.

(a) 0 kG threshold 660 μV
(b) 6 kG threshold 330 μV
(c) 15 kG threshold 330 μV

V = 2050 volts
ΔV = 560 volts

Fig. 14. Spatial resolution as a function of the angle at 4 kG. Threshold is 330 μV, V = 2050 volts, ΔV = 560 volts.

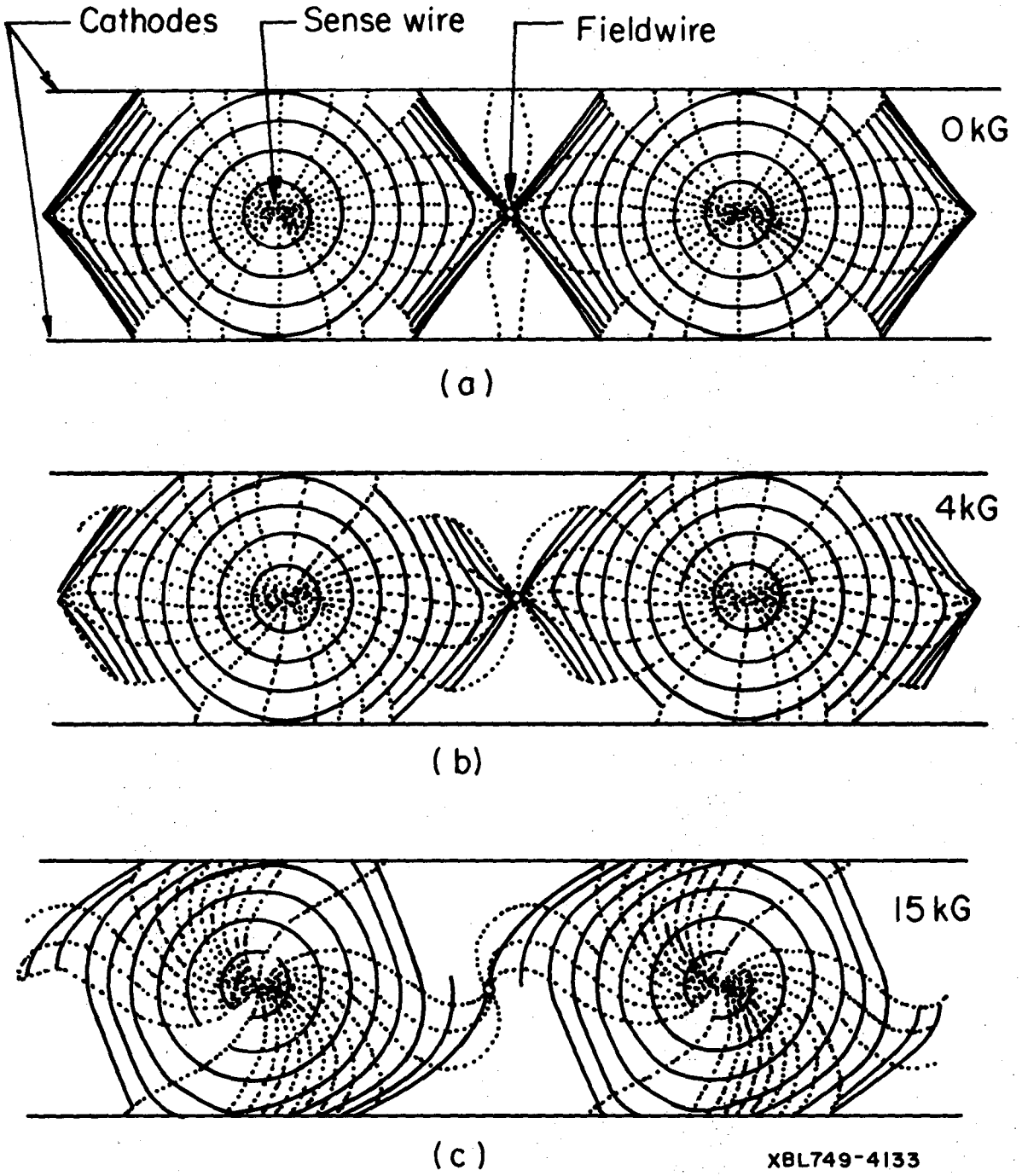

Fig. 1.

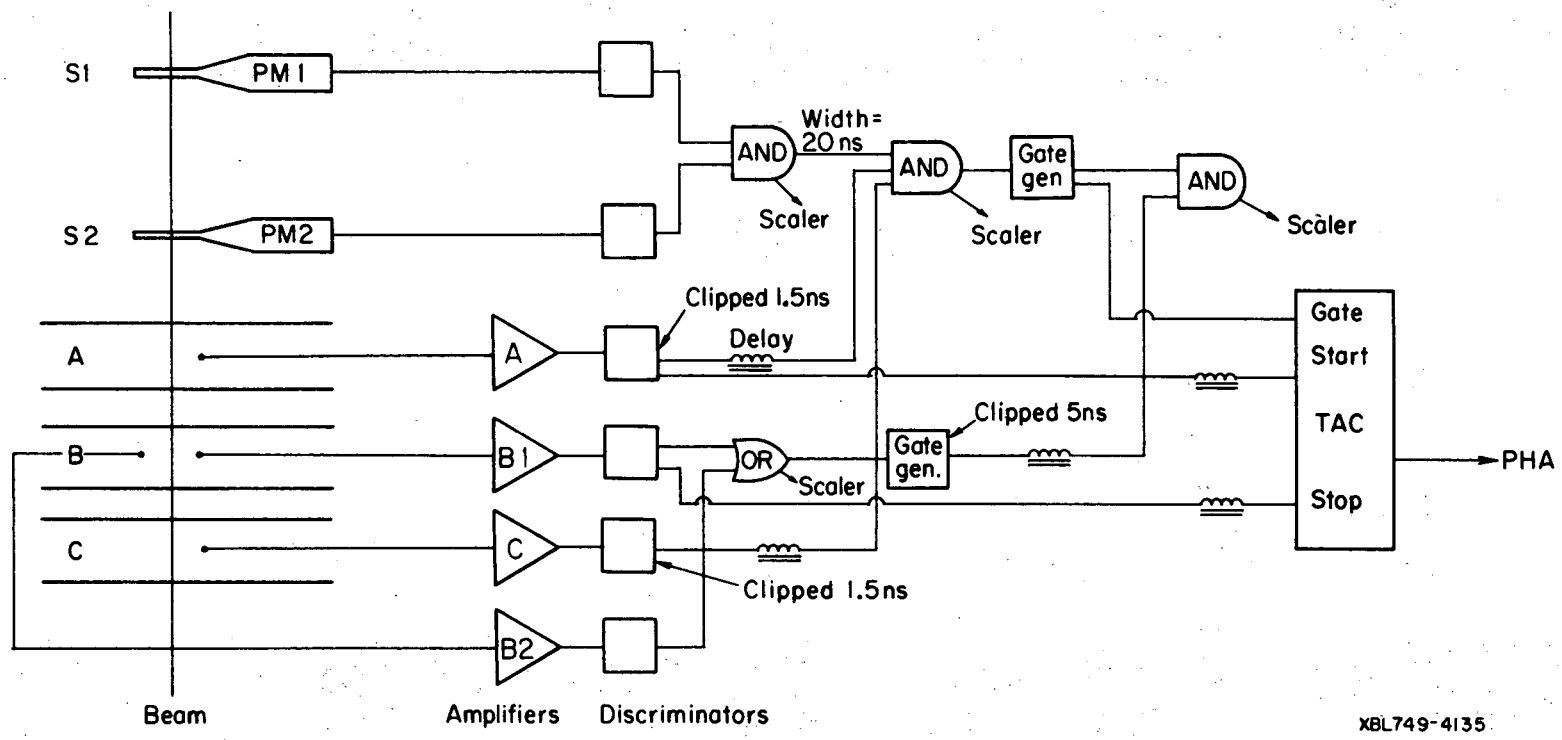
S1
PM 1
S2
PM2
A
B
C
A
B1
B2
Width=
20 ns
AND
Scaler
AND
Scaler
Gate
gen
AND
Scaler
Clipped 1.5ns
Delay
Clipped 5ns
OR
Scaler
Gate
gen.
Clipped 1.5ns
Gate
Start
TAC
Stop
PHA
Beam
Amplifiers
Discriminators
XBL749-4135

Fig. 2.

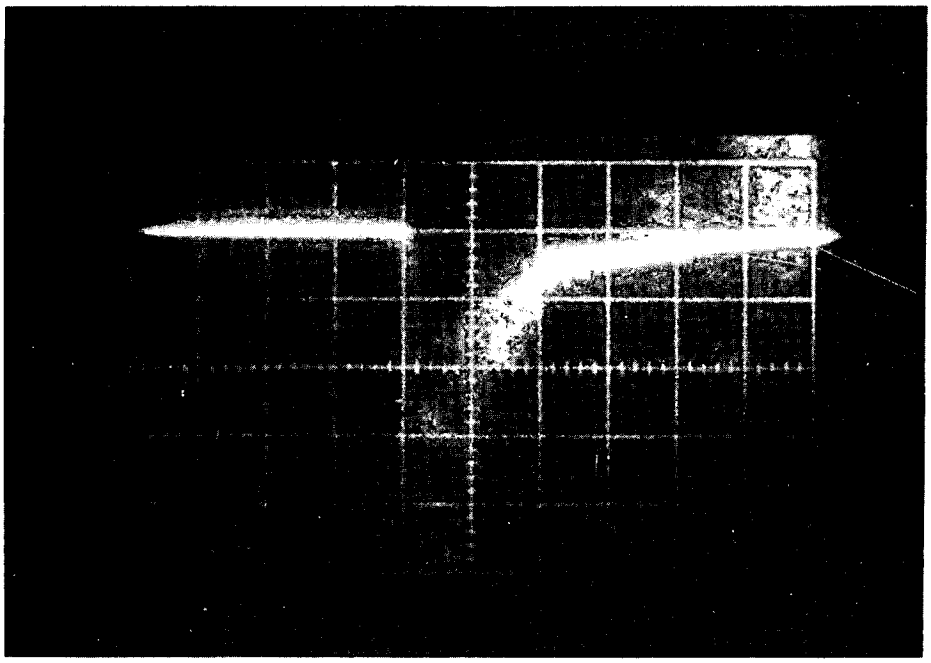

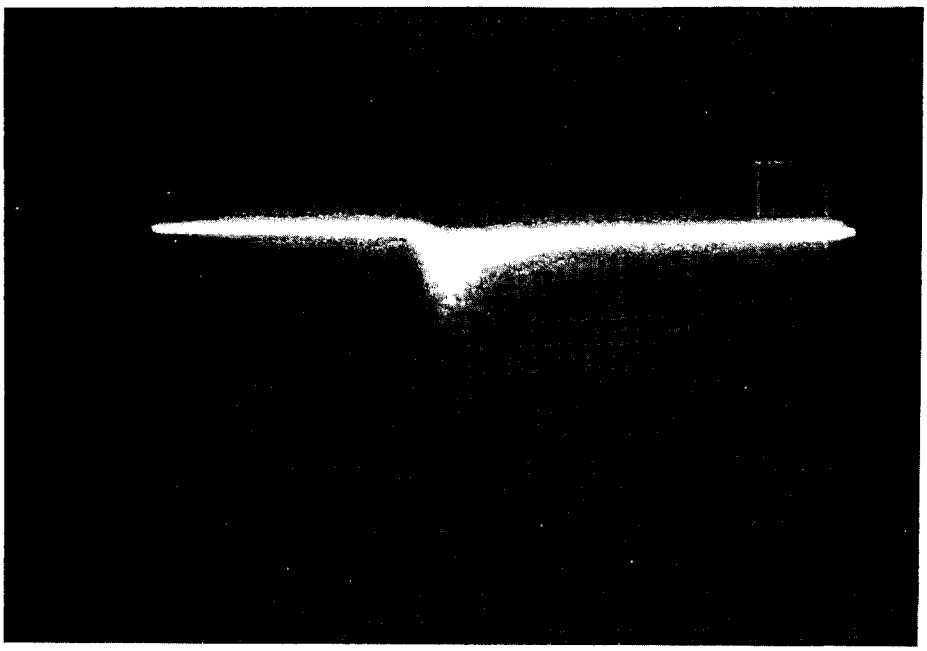

FIG. 3 XBB 749-6229

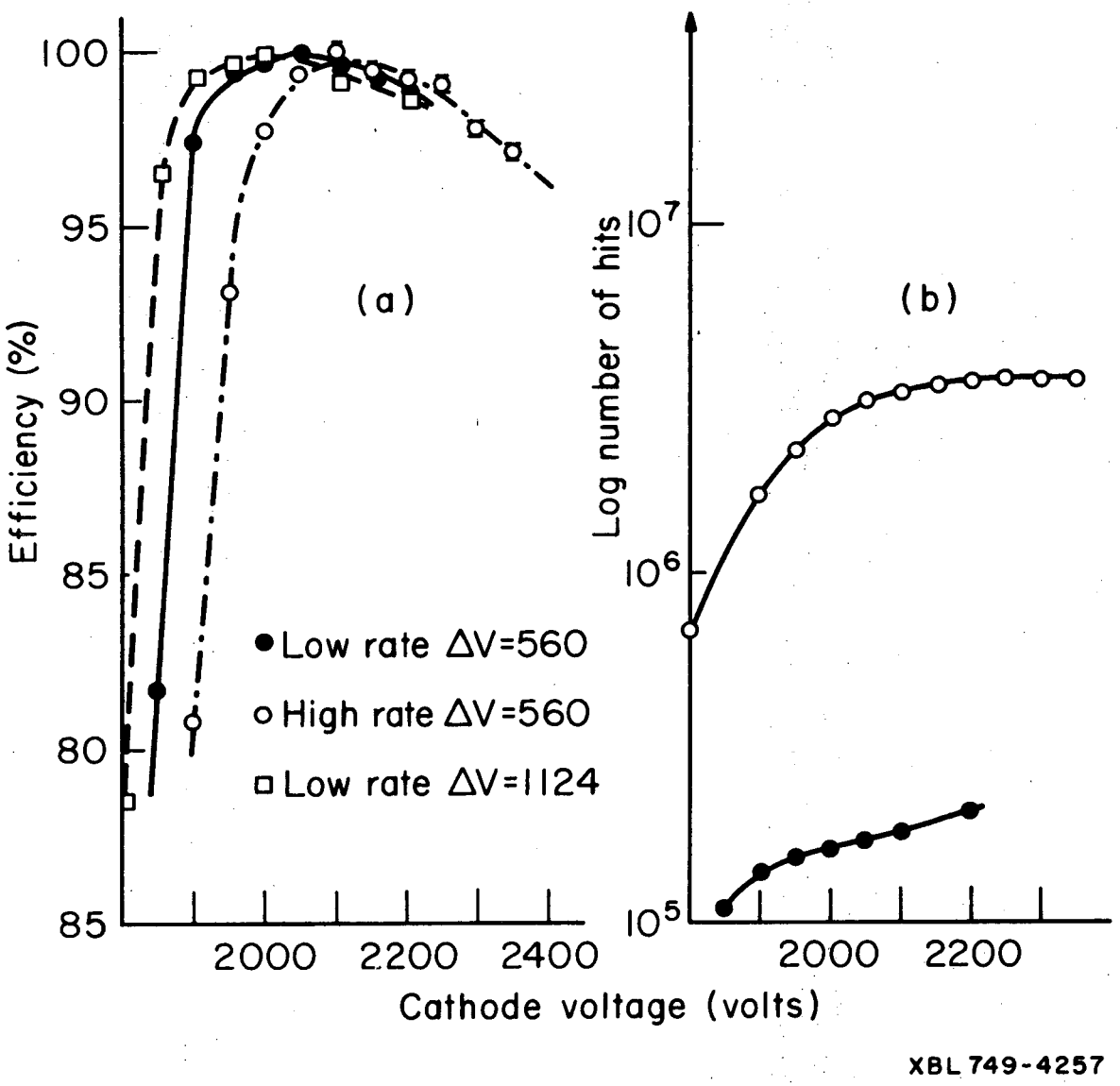
100
95
90
85
80
85
Efficiency (%)
(a)
● Low rate ΔV=560
○ High rate ΔV=560
□ Low rate ΔV=1124
2000
2200
2400
Log number of hits
10^7
10^6
10^5
(b)
2000
2200
Cathode voltage (volts)
XBL 749-4257

Fig. 4.

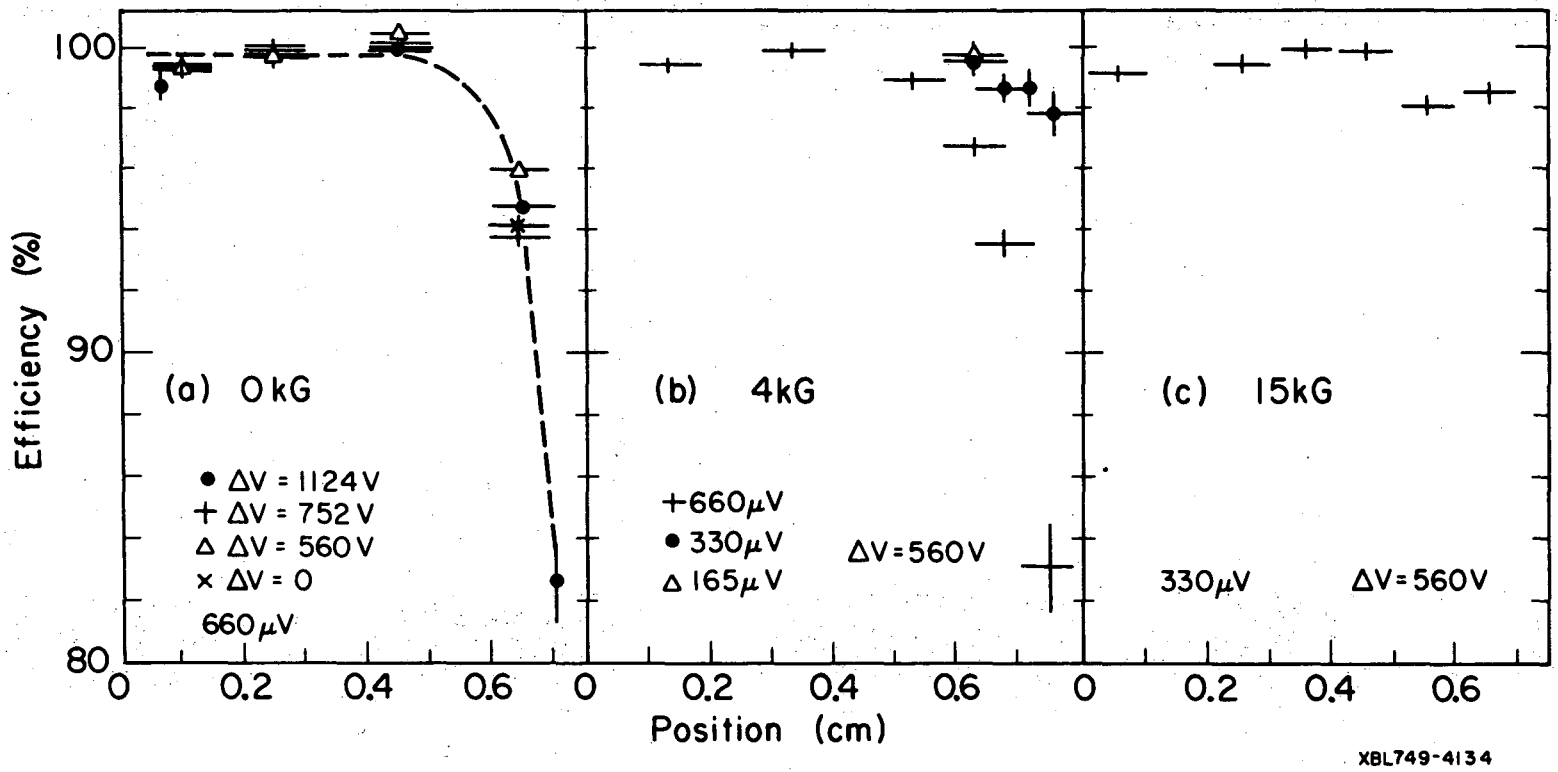
100
90
80
Efficiency (%)
(a) 0 kG
● ΔV = 1124 V
+ ΔV = 752 V
Δ ΔV = 560 V
× ΔV = 0
660 μV
(b) 4kG
+660μV
● 330μV
Δ 165μV
ΔV=560V
(c) 15kG
330μV
ΔV=560V
0
0.2
0.4
0.6
Position (cm)
XBL749-4134

Fig. 5.

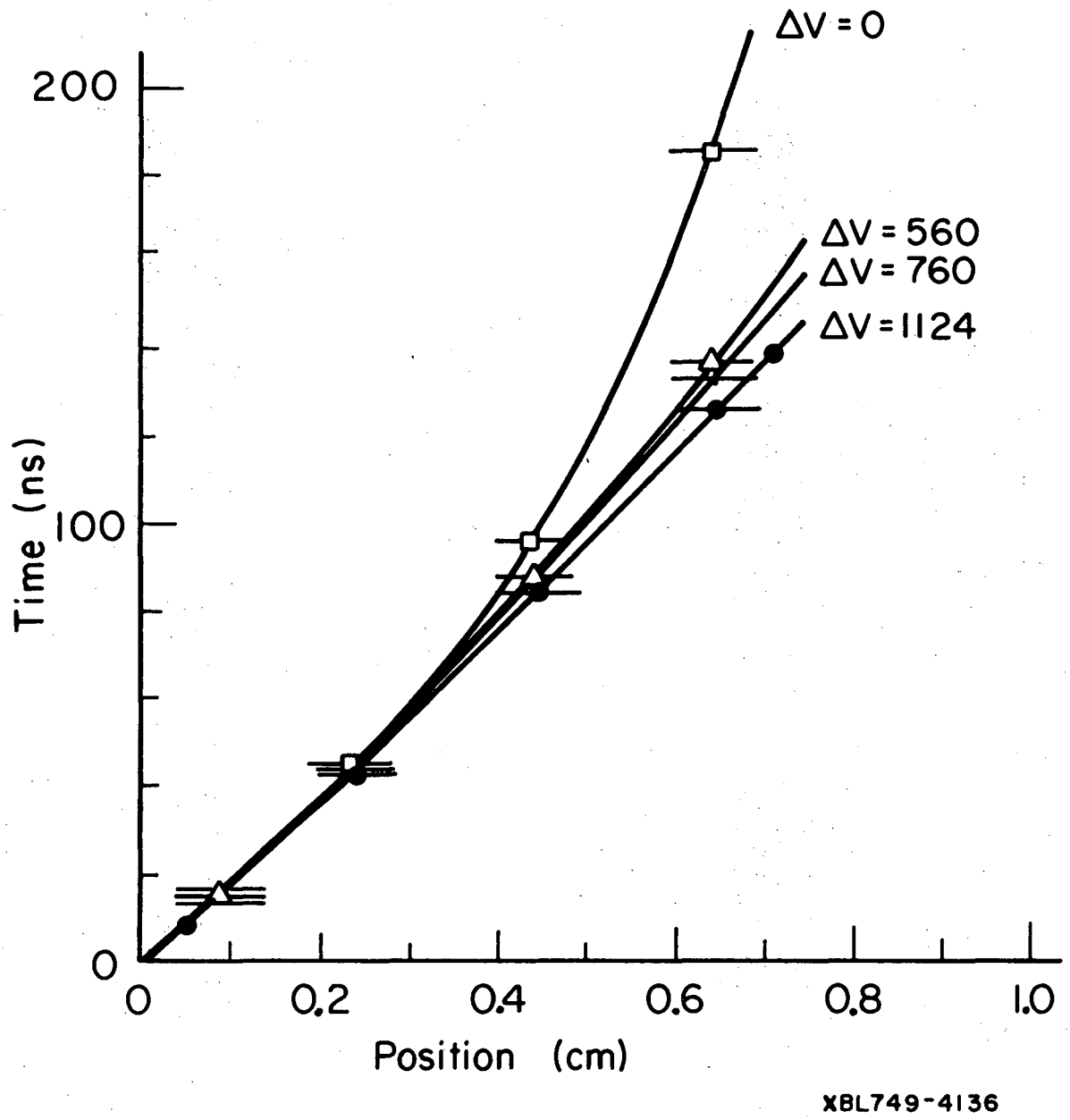
ΔV = 0
ΔV = 560
ΔV = 760
ΔV = 1124
200
100
0
Time (ns)
0
0.2
0.4
0.6
0.8
1.0
Position (cm)
XBL749-4136

Fig. 6.

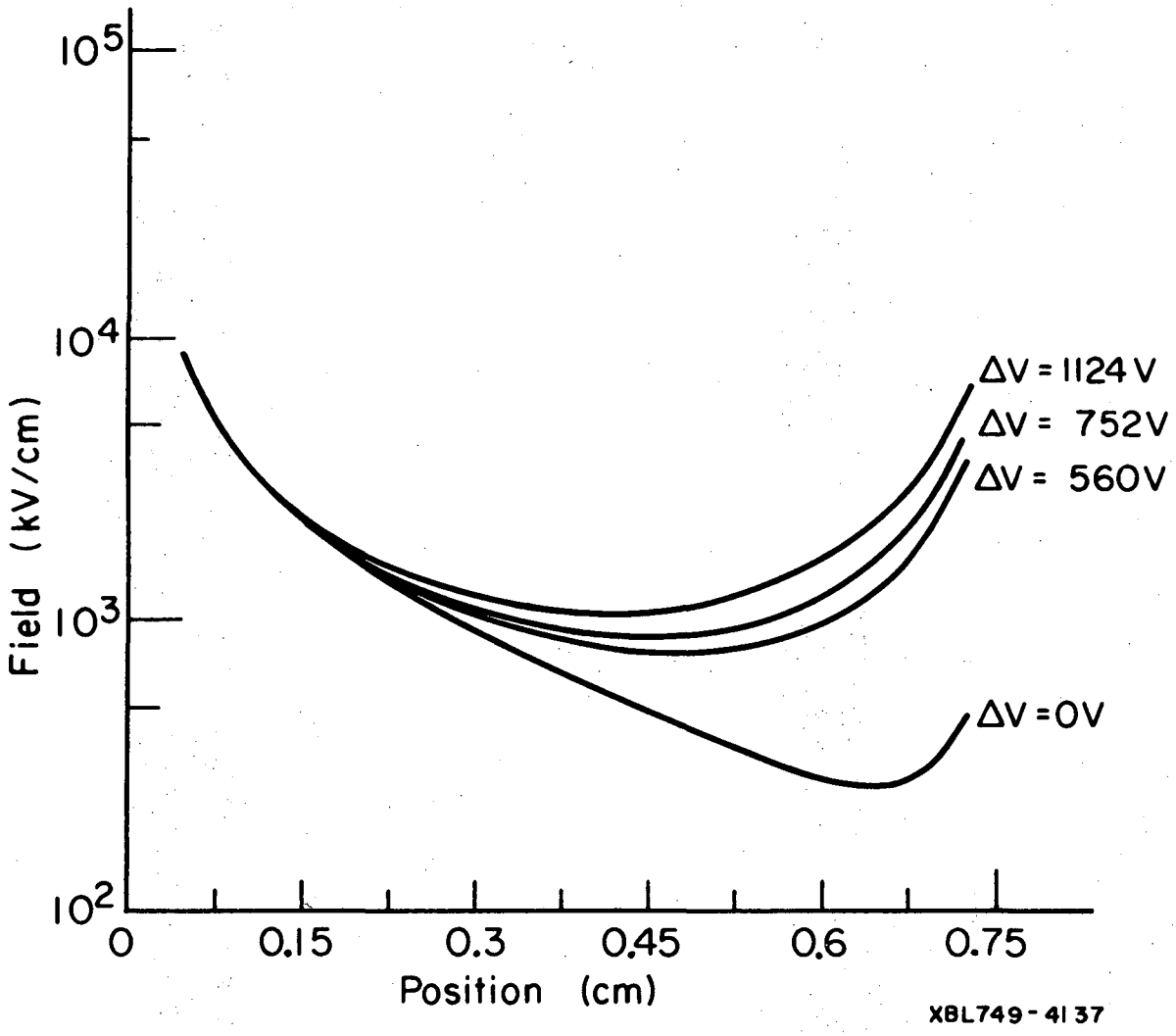
10^5
10^4
10^3
10^2
Field (kV/cm)
ΔV = 1124 V
ΔV = 752V
ΔV = 560V
ΔV = 0V
0
0.15
0.3
0.45
0.6
0.75
Position (cm)
XBL749-4137

Fig. 7.

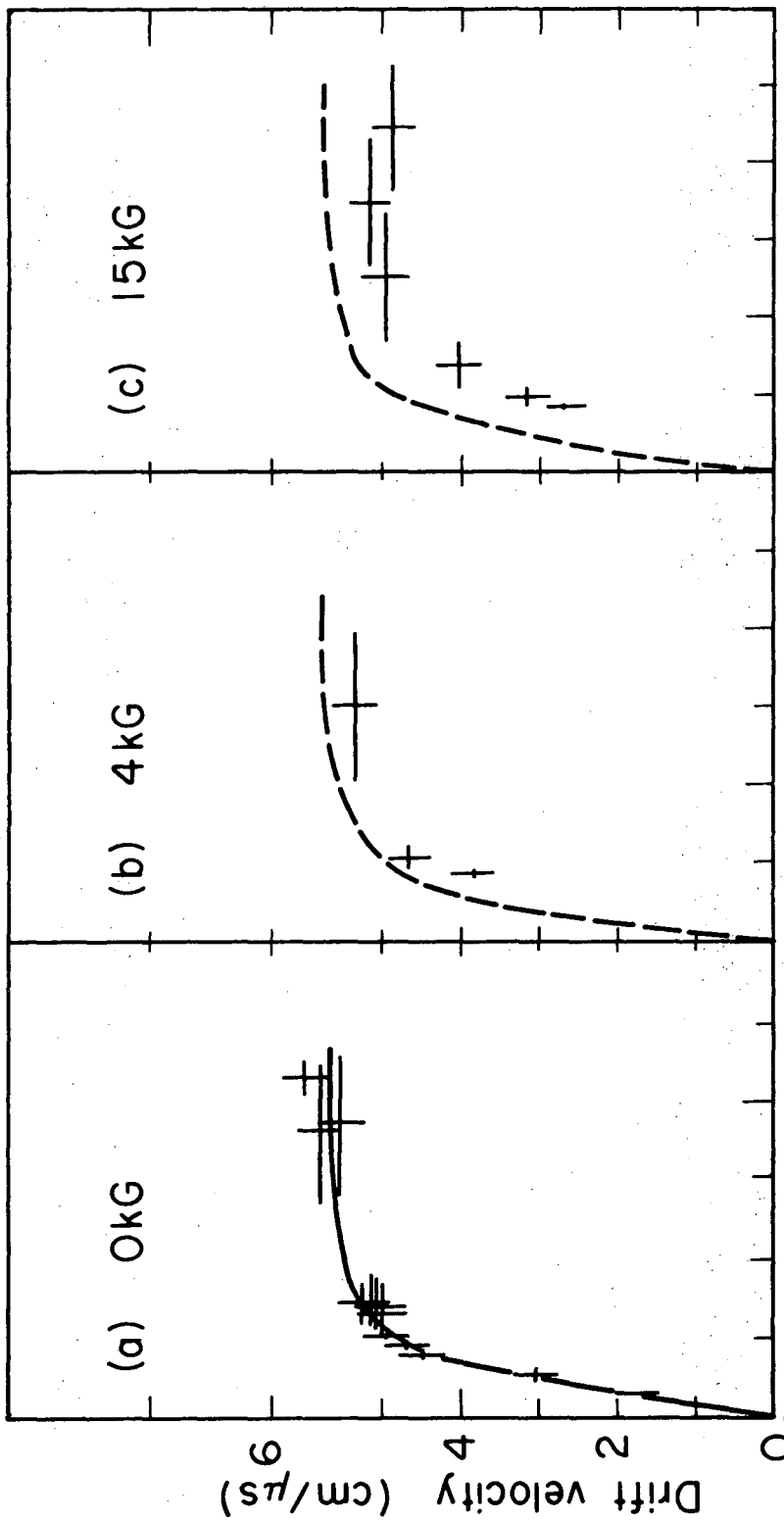

XBL749-4138

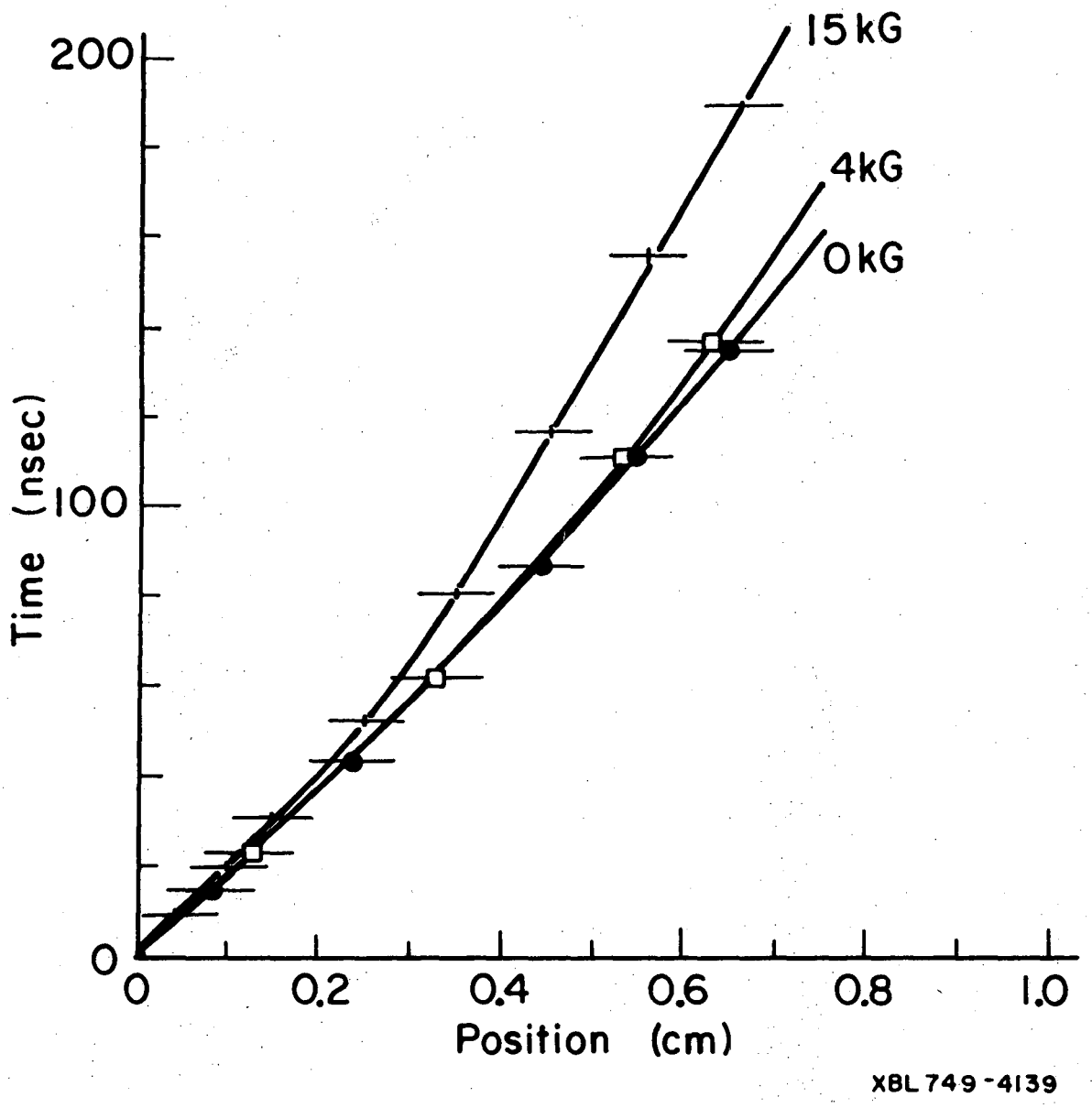
15 kG
4kG
0kG
200
100
0
Time (nsec)
0
0.2
0.4
0.6
0.8
1.0
Position (cm)
XBL 749-4139

Fig. 9.

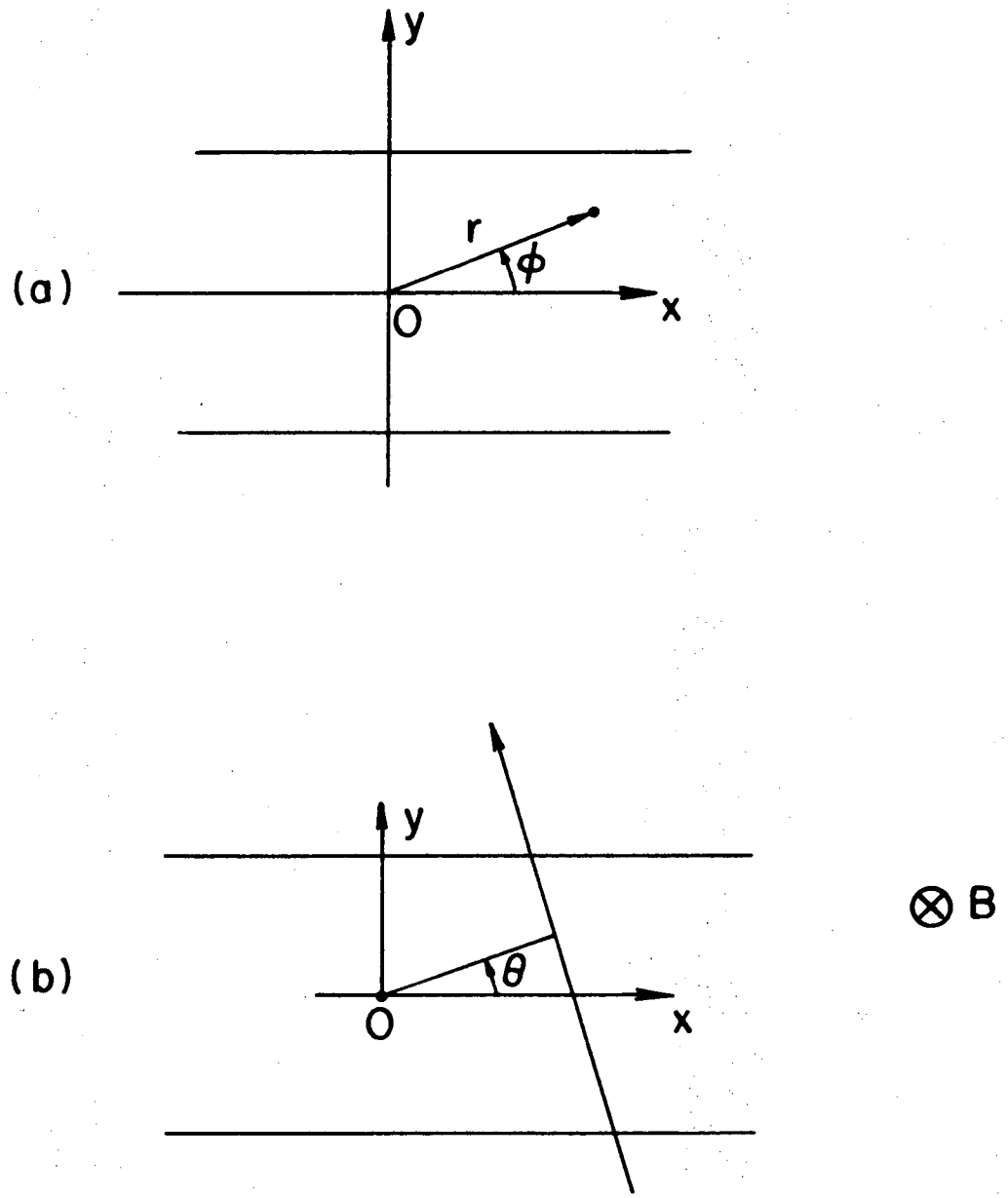

Fig. 10.

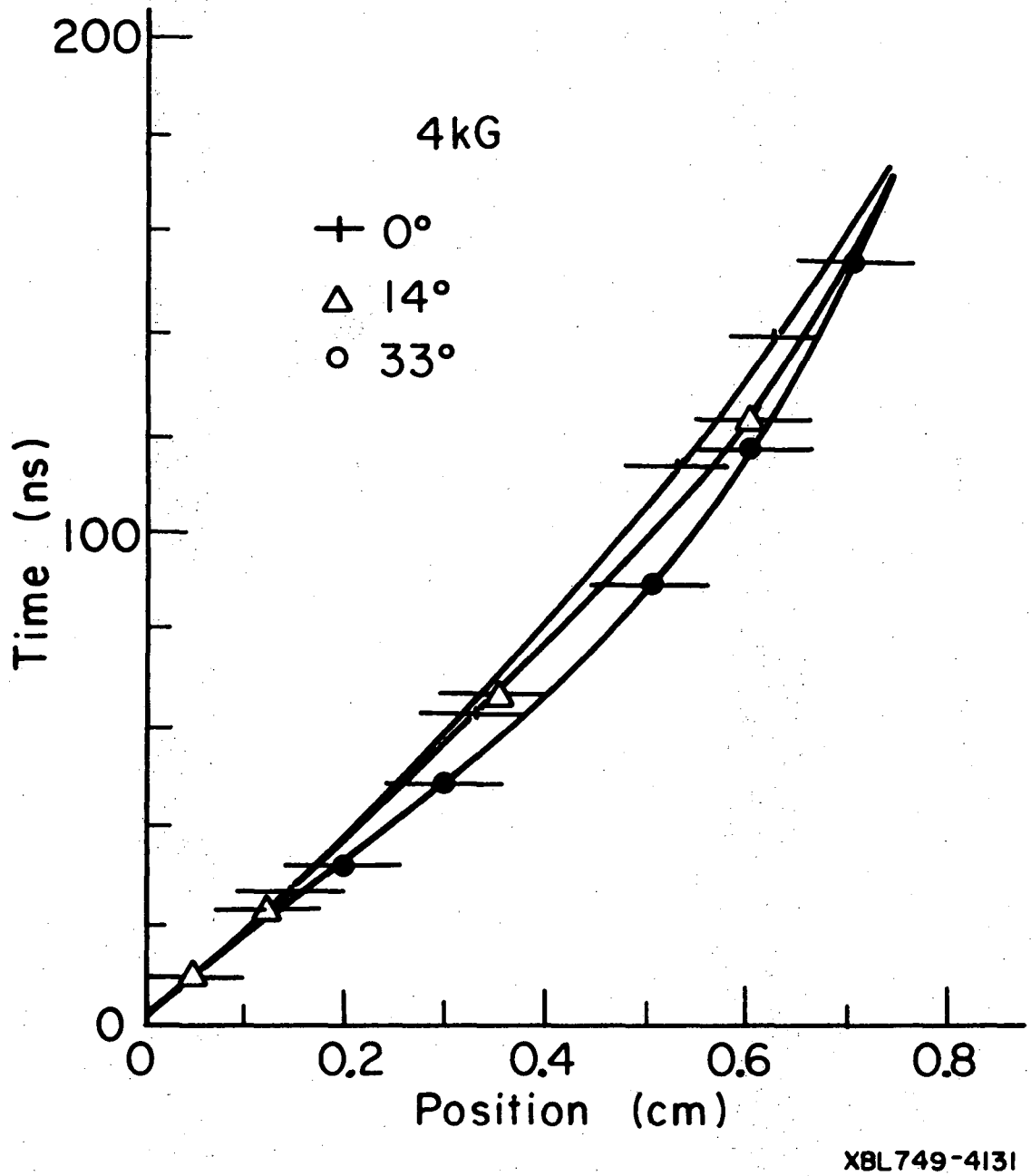
200
100
0
Time (ns)
4kG
+ 0°
Δ 14°
o 33°
0
0.2
0.4
0.6
0.8
Position (cm)
XBL749-4131

Fig. 11.

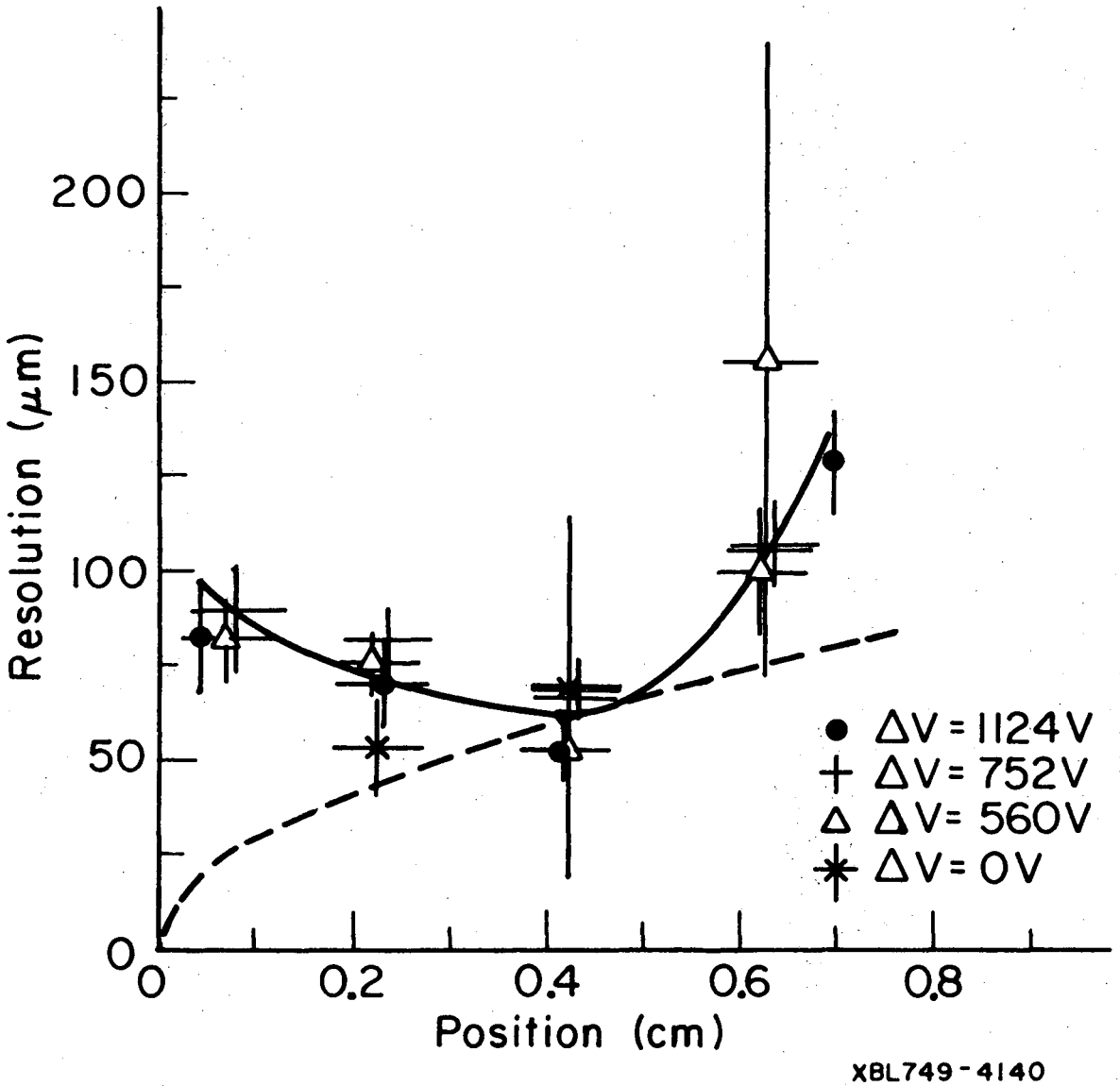
200
150
100
50
0
Resolution (μm)
0
0.2
0.4
0.6
0.8
Position (cm)
ΔV = 1124V
ΔV = 752V
ΔV = 560V
ΔV = 0V
XBL749-4140

Fig. 12.

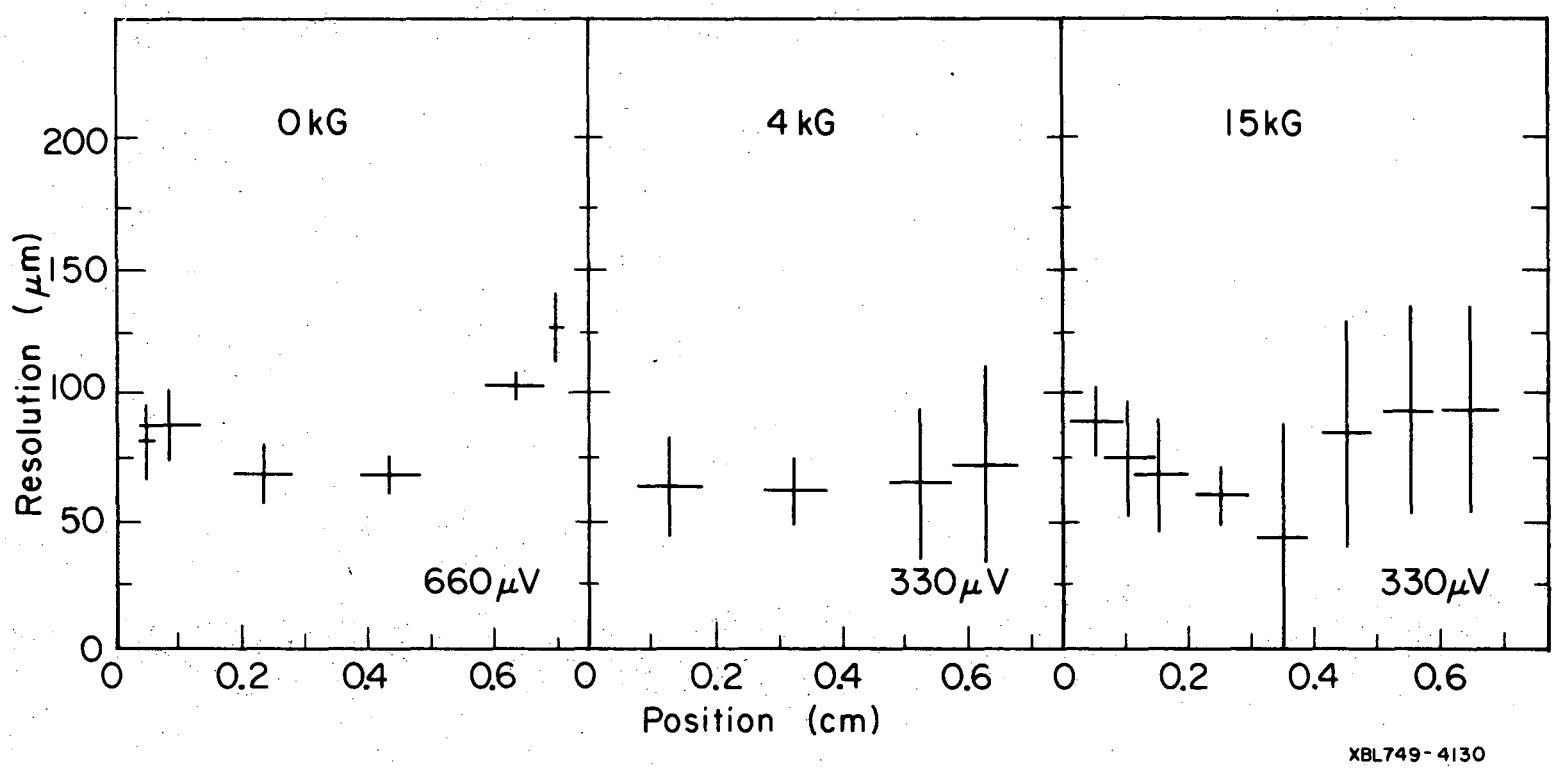
0kG
4kG
15kG
200
150
100
50
0
Resolution (μm)
660μV
330μV
330μV
0
0.2
0.4
0.6
Position (cm)
XBL749-4130

Fig. 13.

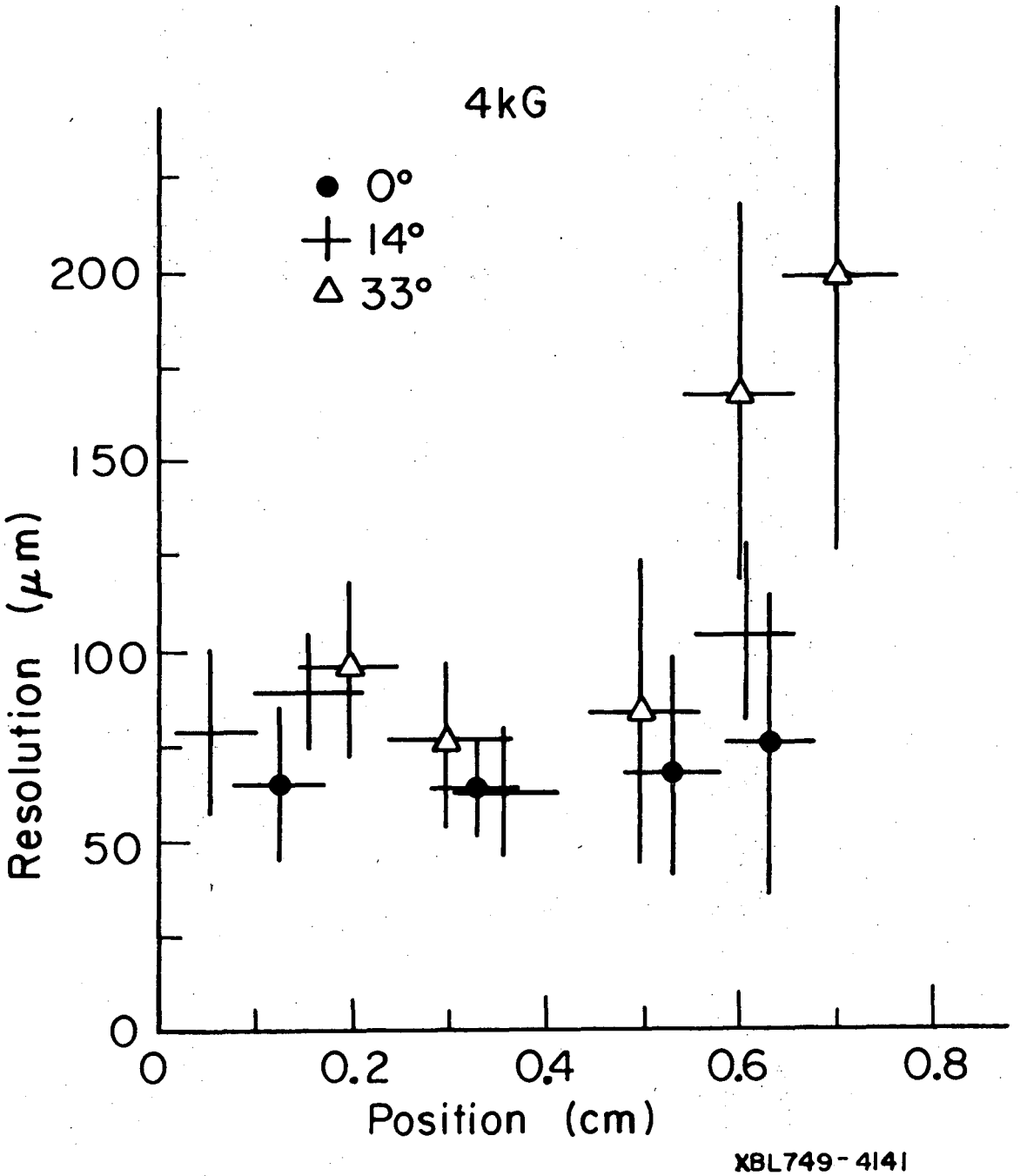
4kG
0°
14°
33°
200
150
100
50
0
Resolution (μm)
0
0.2
0.4
0.6
0.8
Position (cm)
XBL749-4141

Fig. 14.

TECHNICAL INFORMATION DIVISION
LAWRENCE BERKELEY LABORATORY
UNIVERSITY OF CALIFORNIA
BERKELEY, CALIFORNIA 94720